Available online at www.sciencedirect.com
ScienceDirect
Polymer 48 (2007) 720–727
polymer
www.elsevier.com/locate/polymer

Synthesis and characterization of an iron oxide poly(styrene-*co*-carboxybutylmaleimide) ferrimagnetic composite

Selene Sepúlveda-Guzmán [a,*], Lucia Lara [a], Odilia Pérez-Camacho [a], Oliverio Rodríguez-Fernández [a], Amelia Olivas [b], Roberto Escudero [c]

[a] *Centro de Investigación en Química Aplicada, # 460 Blvd. Ing. Enrique Reyna H., CP 25252, Saltillo, Coah, Mexico*
[b] *Centro de Ciencias de la Materia Condensada, Universidad Nacional Autónoma de México, A. Postal 2681, CP 22800. Ensenada, BC, Mexico*
[c] *Instituto de Investigación en Materiales, Universidad Nacional Autónoma de México, A. Postal 70-360, CP 04510, México DF, Mexico*

Received 9 August 2006; received in revised form 25 October 2006; accepted 3 November 2006
Available online 8 January 2007

Abstract

In situ precipitation of iron oxide nanoparticles within the cross-linked styrene-(*N*-4-carboxybutylmaleimide) copolymer was carried out by an ion-exchange method. The resulting composite was studied by X-ray photoelectron (XPS) and Fourier transform infrared (FTIR) spectroscopies. FTIR analysis showed the evolution of iron oxide deposition and the formation of sodium carboxylate due to the deposition treatment. In addition, XPS analysis indicated the complete oxidation of iron(II) to iron(III) by the presence of the representative peaks of iron oxide and iron oxyhydroxide. X-ray diffraction analysis was used to identify the inorganic phases. The results showed the formation of maghemite (γ-Fe_2O_3), and after several deposition cycles, goethite (α-FeOOH). The morphology and spatial distribution of iron oxide particles within the copolymer matrix were determined by transmission electron microscopy. The mean particle size of the iron oxide was of 14 nm as determined from wide-angle X-ray diffraction using the Scherrer equation. The evolution of magnetic properties with the number of deposition cycles was investigated by magnetometry at room temperature. The poly(styrene-*co*-*N*-4-carboxybutylmaleimide)/γ-Fe_2O_3/α-FeOOH/composite showed a soft ferrimagnetic behavior and, after the third deposition cycle, showed a saturation magnetization of 8.04 emu/g at 12 kOe and coercivity field of 51 Oe.

Keywords: Magnetic polymers; Composites; Maleimide copolymers

1. Introduction

In recent years, there has been marked interest in the development of hybrid materials that combine the organic functionality and processability of polymers with the magnetic properties of iron oxide nanoparticles. The polymer/magnetic particle composites have been used in a wide variety of applications such as biological separation systems [1], drug delivery [2], waste water purification adsorbents [3], magnetic resonance markers [4] and different magnetic reprographic methods [5,6].

There are two main methods to prepare polymer/magnetic particle composites. The ex situ method consists of the precipitation of magnetic particles followed by their incorporation into the polymer matrix. Several approaches such as the encapsulation of magnetic particles by the polymer [7], and melt or solution mixture of the polymer, and magnetic particles to form films or fibers [8,9] belong to the ex situ method. On the other hand, in the in situ method the magnetic particles are grown within the polymer matrix. The metal-bonding ability of chelating groups of the matrix is often used to promote the precipitation of the magnetic particles from a metal salt. This method provides an efficient way to control the shape and size distribution of nanoparticles and, unlike inorganic synthetic methods, does not require heating at high temperatures. Several polymers including natural polymers and their derivatives, such as cellulose and carboxymethyl cellulose, have already been used to prepare hybrid materials with magnetic properties by the in situ method [10–12]. Sourty et al. [13] synthesized iron oxide particles using a bacterial cellulose

* Corresponding author. Tel.: +52 844 438 9830; fax: +52 844 438 9463.
E-mail address: ssepulveda@ciqa.mx (S. Sepúlveda-Guzmán).

0032-3861/$ - see front matter © 2007 Elsevier Ltd. All rights reserved.
doi:10.1016/j.polymer.2006.11.004

membrane as matrix, which acts as nucleation site for the crystal growth, and led to a superparamagnetic biomaterial. In a different approach, Ziolo et al. [14] synthesized superparamagnetic γ-Fe_2O_3 nanoparticles within a sulfonated polystyrene matrix. In addition, the use of copolymers with hydrophilic and hydrophobic moieties provides a unique distribution of domains for the precipitation of inorganic nanoparticles [15]. For instance, Ahmed and Kofinas [16] synthesized $CoFe_2O_4$ nanoparticles using a norbornene/norbornene-dicarboxylic acid diblock copolymer as template, by dissolving iron(II) and cobalt(II) chlorides in the polymer solution, which later was cast as a film and oxidized to render the magnetic composite. Copolymers based on maleimides are available with a wide variety of compositions, structures and properties, they are very interesting due to their facile synthesis and desirable thermal properties [17,18]. *N*-Carboxy-maleimide copolymers are able to bind metal ions and have been used in waste water purification systems as ion-exchange resins [19], as adhesion promoters for polymer/metal films [20] and in the construction of multilayer assemblies [21]. In addition, they are excellent polymeric supports of magnetic particles due to their alternating structure. The present work deals with the preparation of magnetic metal oxide particles within a *N*-(4-carboxybutyl)maleimide-styrene cross-linked copolymer by in situ precipitation. Iron oxide deposition was achieved by the adsorption of ferrous ions by the cross-linked copolymer followed by alkaline oxidation with sodium hydroxide. The effect of the chemical treatments on the chemical composition of the composites was studied by spectroscopic techniques such as X-ray diffraction, Fourier transform infrared and X-ray photoelectron spectroscopies. The effect of number of deposition treatments on the iron content and morphology of the iron oxide nanoparticles were studied by atomic absorption and transmission electron microscopy. Magnetometry, zero-field-cooled and field-cooled analyses were done to study the magnetic behavior of the composite.

2. Experimental

2.1. Reagents and materials

Styrene (St, 99%, Aldrich) and divinylbenzene (DVB, 80%, Aldrich) were distilled at reduced pressure before use. *N*-(4-Carboxybutyl)maleimide (CBMi) was prepared by the condensation of maleic anhydride (95%, Aldrich) and aminobutyric acid (99%, Sigma) as reported [22]. Azo-bis-isobutyronitrile (AIBN, 89%, Pflatz & Bauer Inc.) was recrystallized from ethanol. Chloroform (99%, J.T. Backer) was dried by refluxing over phosphorous pentoxide and distilled before use. Ferrous chloride ($FeCl_2 \cdot 4H_2O$, 99%, Aldrich) and sodium hydroxide (NaOH, 97%, Aldrich) were used without further purification. Deionized water was degassed prior to use.

2.2. Synthesis of poly(St-co-CBMi) cross-linked with DVB

Poly(St-*co*-CBMi) cross-linked with 5.0 wt% of DVB was obtained by radical copolymerization in chloroform at 60 °C using AIBN as initiator (Scheme 1). Chloroform (150 mL), St (2.84 g), CBMi (5 g), DVB (0.78 g), and AIBN (0.025 g) were added to a 250 mL three-necked flask equipped with condenser, stirrer and nitrogen inlet. The mixture was degassed and refluxed under a nitrogen atmosphere for 8 h. The residual monomers and initiator were removed by Soxhlet extraction with methylene chloride for 12 h.

2.3. Synthesis of magnetic composite

Poly(St-*co*-CBMi) cross-linked with 5 wt% of DVB (1.5 g), was placed in a solution of $FeCl_2 \cdot 4H_2O$ 0.1 M (150 mL), which had been degassed for 16 h under nitrogen. The cross-linked copolymer was separated by filtration on a fine fritted-glass funnel. The copolymer was washed with copious amounts of deionized water until no iron was detected in the eluent by the thiocyanate test [23]. Then, the cross-linked copolymer was dispersed in a solution of 4.0 N NaOH (60 mL), purged with nitrogen, heated to 70 °C and stirred for 4 h. The mixture was cooled and filtered to remove the composite, which was then washed thoroughly with deionized water until the pH was neutral. The modified cross-linked copolymer was dried by freeze drying. The deposition treatment was repeated up to four times to increase the amount of iron oxide within the cross-linked copolymer.

2.4. Characterization

Infrared spectra were recorded as KBr pellets using a *IR Nicolet Gemini Magna 550 C*. The samples were also analyzed by X-ray photoelectron spectroscopy (XPS) on a modified laser ablation system, *Riber LDM-32*, using a *Cameca Mac3* analyzer. The X-ray Al Kα line at 1486.6 eV was used for excitation. Wide-scan photoelectron spectra were collected by acquiring data for every 1.0 eV with an energy resolution of 3 eV. Narrow-scan photoelectron spectra were recorded for C 1s, N 1s, O 1s, Na 1s and Fe 2p by acquiring data for every 0.2 eV and the energy resolution was 0.8 eV. In addition, charging effect was corrected by shifting the binding energies considering the C 1s signal at 285 eV. Nonlinear fit, using Gaussian curves was performed by maintaining the full-width at half-maximum (FWHM) constant for all components in a particular spectrum. Surface atomic concentration ratios were calculated from the peak areas, using reported sensitivity factors [24]. Elemental analysis was done using a Perkin–Elmer CHN S/O 2400. Iron content within the composite was obtained by atomic absorption analysis using a *Varian Spectra A-250 plus* spectrophotometer. X-ray diffractograms were recorded using a *Siemens D-5000* diffractometer with Cu Kα radiation at 35 kV and 25 mA at a scan rate of 0.03° (2θ)/s. Transmission electron micrographs were taken using a *JEOL 2010* microscope with an atomic resolution of 0.19 nm. Before the analysis, the samples were sonicated in deionized water and deposited on carbon film copper grids (400 mesh). Magnetization curves were acquired using a *Lake Shore 7300* vibrating sample magnetometer with a maximum field of 15 kOe. Zero-field-cooled (ZFC) and field-cooled (FC) analyses were

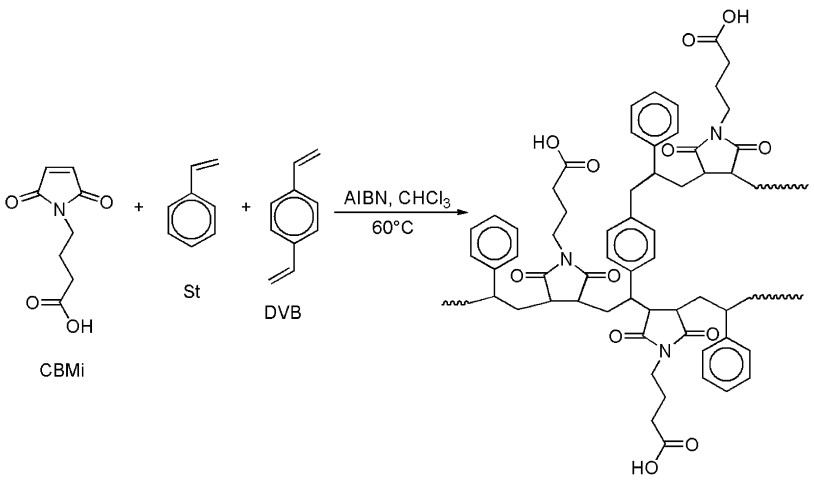

Scheme 1. Synthesis of poly(St-*co*-CBMi) cross-linked with DVB.

carried out in a SQUID (superconducting quantum interference device) *MPMS* magnetometer from *Quantum Design*.

3. Results and discussion

3.1. Synthesis of magnetic composites

Poly(St-*co*-CBMi) cross-linked with DVB was synthesized by radical polymerization (Scheme 1). We previously reported the tendency to form alternating structures by radical copolymerization of CBMi with St without cross-linking [25]. The synthesis of the cross-linked copolymer showed a very similar tendency to that observed for linear St-CBMi copolymer; it is consistent with the maleimide content and the conversion data for the cross-linked copolymer. During the iron oxide deposition by in situ treatment, ferrous ions were introduced by swelling the cross-linked copolymer powder in a ferrous chloride solution. In this stage, the cross-linked copolymer became yellow due to absorption of iron(II) ions. The addition of sodium hydroxide solution led to precipitation of $Fe(OH)_2$ followed by formation of iron oxide, as indicated by the successive change in color of the copolymer to green and then to dark brown [14,26,27]. No color changes in the composite were observed after the second deposition cycle, due to darkening of the sample.

3.2. Chemical characterization

The FTIR spectra of poly(St-*co*-CBMi) cross-linked with DVB and the composite after each deposition cycle are shown in Fig. 1. Characteristic absorption bands of the functional moieties of CBMi and St are displayed in the FTIR spectrum of the cross-linked copolymer (Fig. 1a). The C–N–C and C=O stretching vibrations at 1405 cm^{-1} and 1695 cm^{-1} are associated with the imide and carbonyl groups, respectively [28]. In addition, aromatic C–H out-of-plane bending vibration at 700 cm^{-1} and aromatic C–C stretching vibrations at 1450 cm^{-1} and 1140 cm^{-1} are also observed [29]. The presence of a peak associated with the asymmetric stretching of the carboxylate groups at 1550 cm^{-1} and the considerable decrease in the intensity of the carboxylic acid stretching vibration at 1695 cm^{-1} (Fig. 1b), indicate that after the iron oxide deposition process, the carboxylic groups (COOH) in the cross-linked copolymer changed to sodium carboxylate groups (COONa) due to their reaction with NaOH. The presence of iron oxide after the second deposition cycle was supported by two new peaks at 476 cm^{-1} and 570 cm^{-1}, associated with Fe–O bending vibrations of the maghemite iron oxide phase [30]. In addition, two peaks at 896 cm^{-1} and 794 cm^{-1} were observed after the third deposition cycle, which are assigned to in-plane and out-of-plane Fe–O–OH bending vibrations in goethite [31]. These absorption peaks suggest the presence of a mixture of iron oxide phases in the cross-linked copolymer after four deposition cycles. This change is accompanied by an increase in the hygroscopicity of the sample, due to the

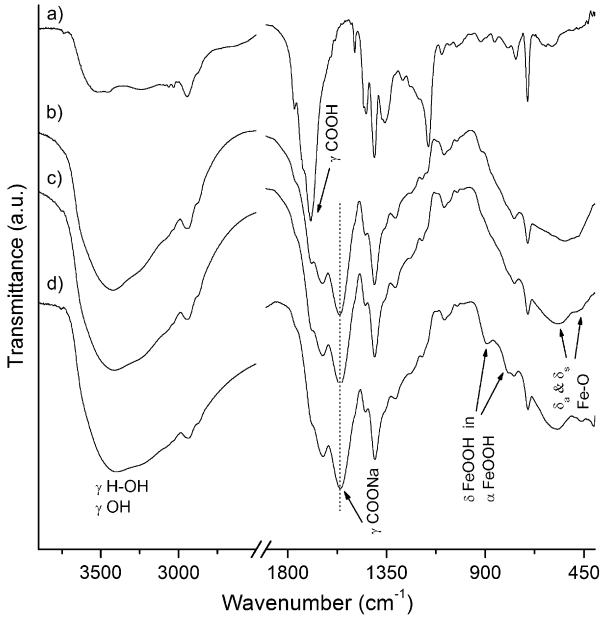

Fig. 1. (a) FTIR spectra of the cross-linked copolymer and composite obtained after (b) one, (c) two and (d) three chemical deposition cycles.

sodium carboxylate groups and iron oxide particles, as evidenced by the intense band at ~3330 cm^{-1} due to O–H stretching vibrations.

In order to determine the iron oxide phase deposited in the cross-linked copolymer after each cycle, the samples were analyzed by XRD techniques (Fig. 2). Due to the large polymer fraction in the composite after the first deposition cycle, the scattering spectrum shows only an amorphous halo (Fig. 2a). However, after the second deposition cycle, the iron oxide within the composite could be identified as γ-Fe_2O_3 (maghemite) (Fig. 2b) [32]. After the third deposition cycle, the diffraction pattern of the composite showed a low contribution of another iron oxide phase identified as α-FeOOH (goethite) (Fig. 2c) [32]. The precipitation of maghemite after each cycle of treatment takes place at a relatively low temperature (70 °C) [14]; however, when the cross-linked copolymer was treated for four times, the goethite phase was the main iron oxide phase in the composite, possibly due to maghemite oxidation during the subsequent treatments [33]. These observations are consistent with the analyses of the composite by FTIR where the inorganic phase consists of two phases of iron oxide and also suggest that the process to obtain selective magnetic phases is difficult and agree with others' reports [34].

In this study, XPS analyses were done to monitor the iron oxide deposition in the cross-linked copolymer. The wide-scan spectra of the cross-liked copolymer, showing the C 1s, O 1s, and N 1s core-level peaks, are shown in Fig. 3a. However, after four deposition cycles, the wide-scan spectrum of the composite exhibits two more peaks associated with Na and Fe, due to the sodium carboxylate in the cross-linked copolymer and the iron oxide deposition (Fig. 3d). In both cases, the cross-linked copolymer and the composite spectra, carbon and oxygen peaks exhibit the higher intensities. High-resolution scans for C 1s and O 1s peaks from the cross-linked copolymer are shown in Fig. 3. The maleimide copolymers have been scarcely studied by XPS. The deconvolution of the C 1s core-level spectrum of the cross-linked copolymer was fitted to five peaks at 284.1 eV (*C*–COOH), 284.9 eV (alkyl-C, aromatic-C), 285.9 eV (imide C–H), 287.2 eV (C=O, carboxylic acid) and 289 eV (C=O, imide). Peak assignment was based on characteristic binding energies from the literature [28,35,36] and agrees well with the structure of poly(St-*co*-CBMi). Moreover, the O 1s core-level spectra of the cross-linked copolymer were fitted using two peaks at 532.3 eV and 534 eV (Fig. 3c). The first one associated with the binding energy of the C=O in the imide group and carboxylic acid group and the second one at the bending energy of the OH in the carboxylic acid group [28,35,36]. In addition, after correction with sensitivity factor the N/C ratio measured by XPS was 0.05; this value is consistent with the maleimide content calculated from elemental analyses.

The high-resolution spectra of the C 1s and O 1s core-level collected from the resulting composite are shown in Fig. 3e and Fig. 3f, respectively. After the fourth deposition cycle, the deconvolution of the C 1s core-level spectrum was fitted with four peaks at 283.6 eV (*C*–COONa), 284.8 eV (alkyl-C, aromatic-C), 285.9 eV (imide C–H) and 288 eV (C=O, imide). The absence of the peak at 287.2 eV, associated with the bending energy of carboxylic acid groups, is accompanied by an increase in the intensity of the peak at 285.9 eV, due to the contribution of the carboxylate species [36] in the cross-linked copolymer. These groups were also observed by the FTIR analysis. The O 1s core-level spectrum from the resulting composite was fitted to five peaks at 530.2 eV (α-FeOOH, γ-Fe_2O_3), 531.4 eV (α-FeOOH, (C=O)–ONa), 532.6 eV ((C=O)–N), 534 eV (H_2O) and 536 eV (Na KVV). The intensity of the peak assigned to the binding energy of carbonyl groups (532.5 eV) decreased due to the absence of carboxylic acid groups. In addition, a new peak associated with binding energy of the carboxylate groups at 531.4 eV was also observed [36]. The presence of water and the Na KVV peaks is due to the hygroscopicity and the sodium carboxylate of the resulting composite, respectively [36]. Moreover, the spectrum displays two peaks associated with the iron oxide in the composite, which are in good agreement with the goethite, at 530.3 eV and 531.4 eV [37] and with maghemite displays one peak at 530 eV [38]. The high-resolution Fe 2p spectrum of the composite after four deposition cycles is shown in Fig. 4. The Fe 2p spectrum provides result that confirmed the complete oxidation of iron(II) to iron(III) after exposure to sodium hydroxide. The deconvolution shows two peaks due to spin–orbit splitting associated with the bending energy of the

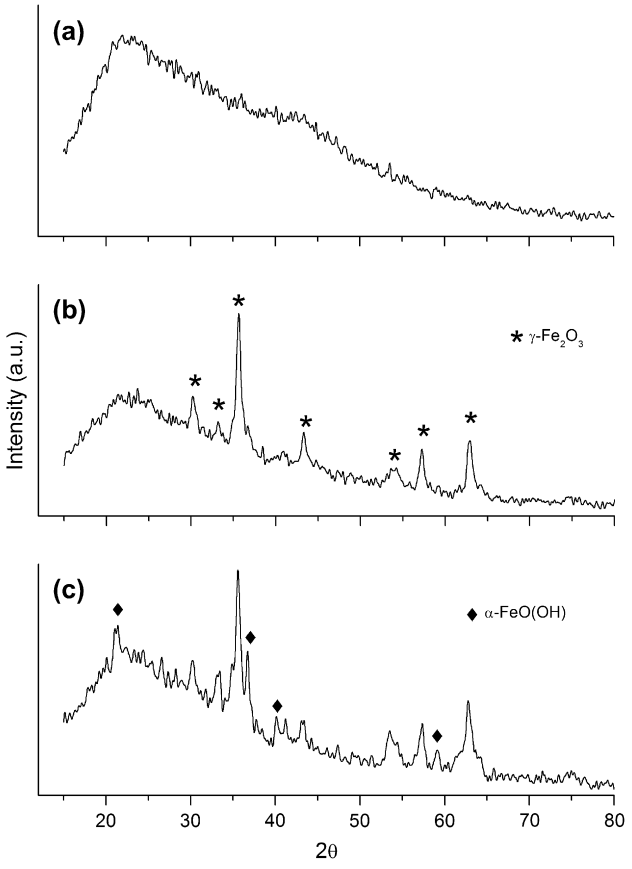

Fig. 2. Wide-angle X-ray diffraction patterns of the composites with (a) one, (b) two and (c) three cycles of treatment.

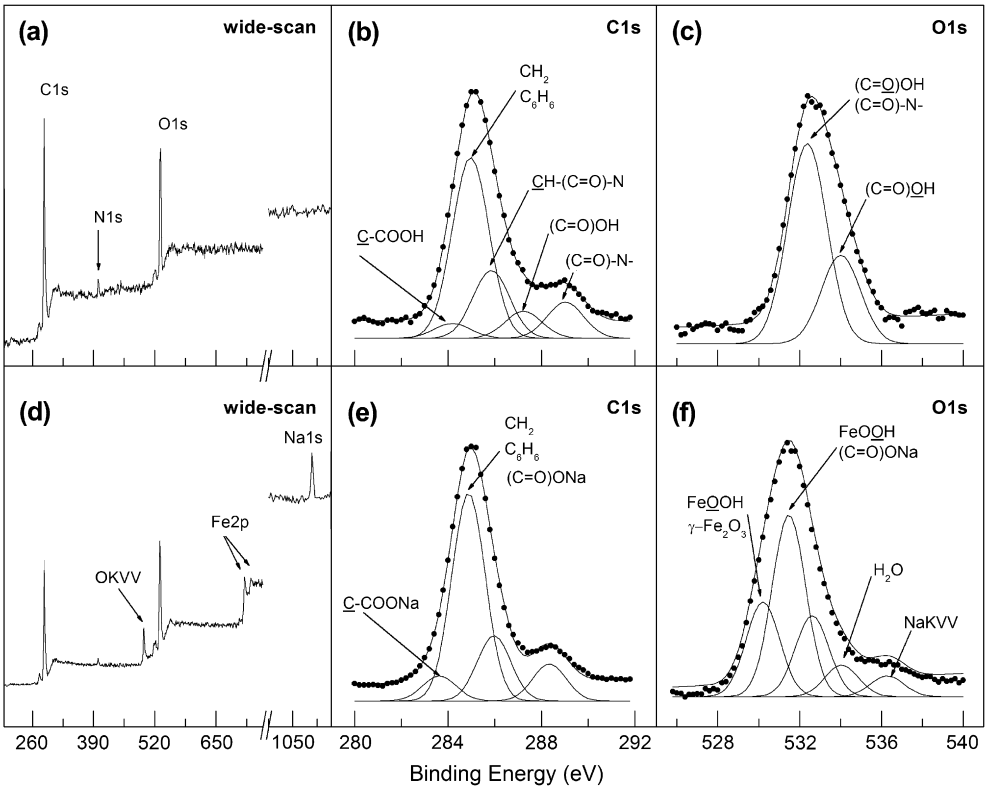

Fig. 3. (a) Wide scan, (b) C 1s and (c) O 1s spectra of the cross-linked copolymer and (d) wide scan, (e) C 1s and (f) O 1s spectra of the composite after four deposition cycles.

Fe^{3+} at 711.8 eV for Fe $2p_{3/2}$ and at 725.2 eV for Fe $2p_{1/2}$, due to the maghemite and goethite phases. In addition, two peaks associated with shake up lines for metal transitions at 715.8 eV and 720.1 eV were also observed [24].

3.3. Iron oxide content analysis

The iron content incorporated into the composite with the number of deposition cycles is shown in Fig. 5. The amount of iron increased with the number of deposition cycles; however, a positive deviation from linearity is observed, possibly due to the change from carboxylic acid to sodium carboxylate groups caused by the chemical treatment during the deposition cycles. In order to support this, the iron content was determined after one deposition cycle within the sample of cross-linked copolymer containing carboxylic acid groups and other containing sodium carboxylate groups. The former showed a lower iron content (0.52 wt%) compared to the latter (4.67 wt%). The difference can be explained by the differences in the ionization, since in aqueous media the ionization of COONa groups is considerably higher than those of COOH groups [39]. In addition, after the second deposition cycle, the previously deposited iron oxide particles act as deposition point for iron(II) ions, resulting in an autocatalytic deposition mechanism [37]. This is further supported by the drastic increase of iron in the composites, from 11 wt% after the third, to 28 wt% after the fourth deposition cycle.

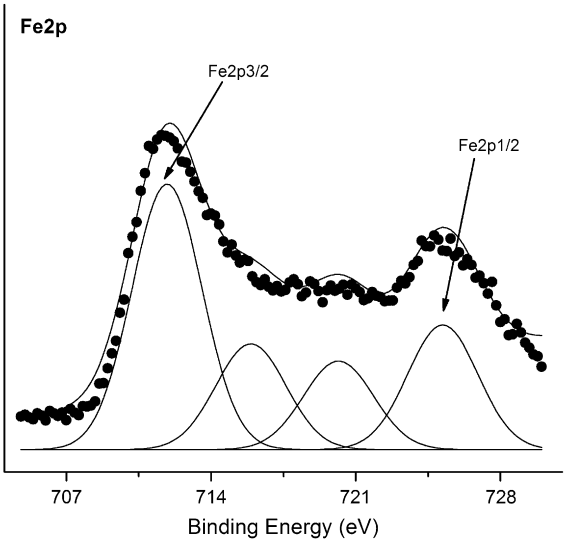

Fig. 4. Fe 2p spectrum of the composite after four deposition cycles.

3.4. Morphology of the composite

The mean particle size after each deposition cycle was calculated by the Scherrer equation using the XRD diffractograms [40]. The results show that the mean particle size within the matrix after two, three and four deposition cycles was 14 nm. These results suggest that the iron oxide particle growth is limited by the cross-linked copolymer, and after each deposition cycle new particles are formed while the average size

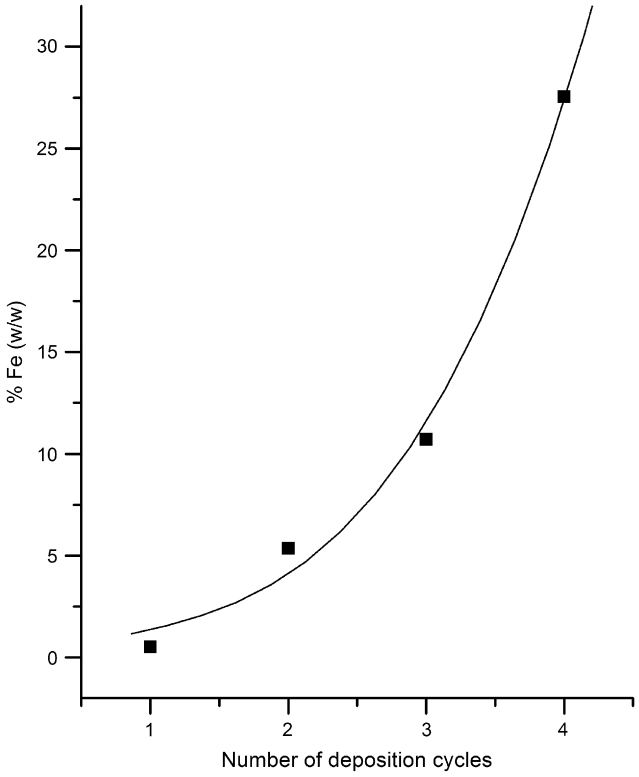

Fig. 5. Iron content incorporated with the number of deposition cycles.

remains constant. These observations are in agreement with those reported earlier for the dependence of the particle size with the number of deposition cycles for other composites [41]. The morphology was studied by TEM; micrographs are shown in Fig. 6. After three deposition cycles, the composite showed a higher number density of maghemite particles with spherical shape (Fig. 6a). However, after four cycles, the particle number density increased leading to the formation of aggregates (Fig. 6b). These observations are due to subsequent precipitation of the iron oxide in the polymer by the functional groups in the cross-linked copolymer and were consistent with the iron content analysis. After the third deposition, the deposited iron oxide particles presumably act as a nucleation site leading to the formation of the observed aggregates. In addition, the formation of iron oxyhydroxide, such as goethite, is associated with aggregates of colloidal particles [42] and is consistent with the results of XRD, which showed goethite as the main iron oxide phase after the fourth deposition cycle.

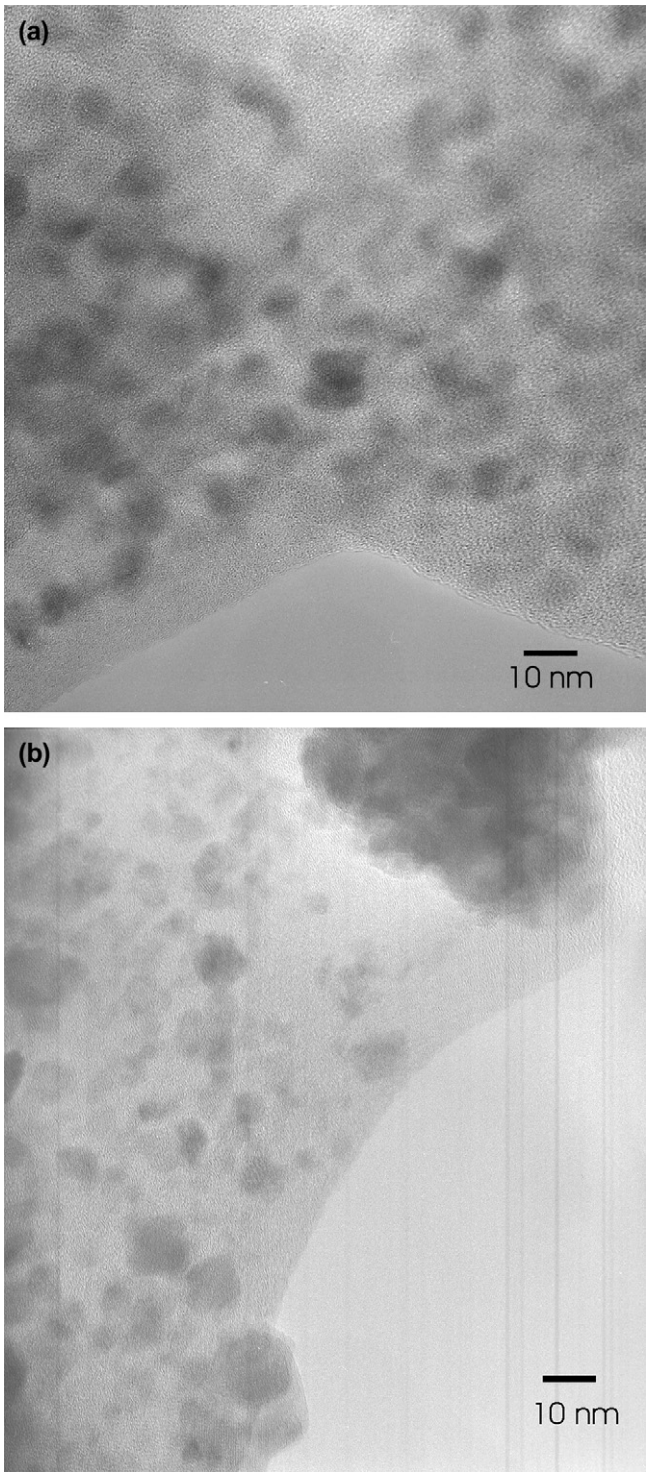

Fig. 6. TEM micrographs of the composite after (a) three and (b) four deposition cycles.

3.5. Magnetic properties of the composite

The magnetic properties of the composites were studied by magnetization measurements in zero-field-cooled (ZFC) and field-cooled (FC) analyses. The magnetization curve of the resulting composite after the fourth deposition cycles shows a soft ferrimagnetic behavior, with a magnetization of 8.04 emu/g at 12 kOe and coercivity field of 51 Oe (Fig. 7). The Fig. 7 inset shows an increase in the magnetization of the composite with the numbers of deposition cycles due to subsequent iron oxide deposition. However, after the fourth cycle the magnetization remains constant due to the low contribution of the magnetization of the goethite phase [43]. In addition, magnetization curves at different temperatures of the composite after the fourth deposition cycle are shown in the Fig. 8. The composite showed a soft ferrimagnetic behavior in the analyzed temperature range and the coercivity field decreased with the

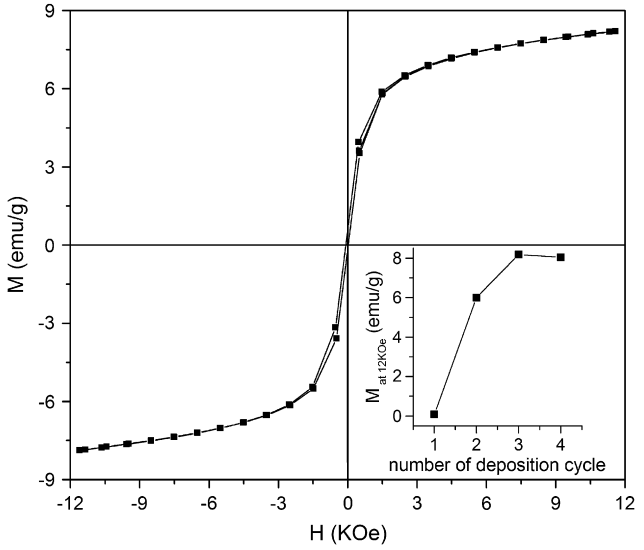

Fig. 7. Room temperature magnetization curve of the composite after four deposition cycles. Inset: change in the magnetization at 12 kOe of the composite with the number of deposition cycles.

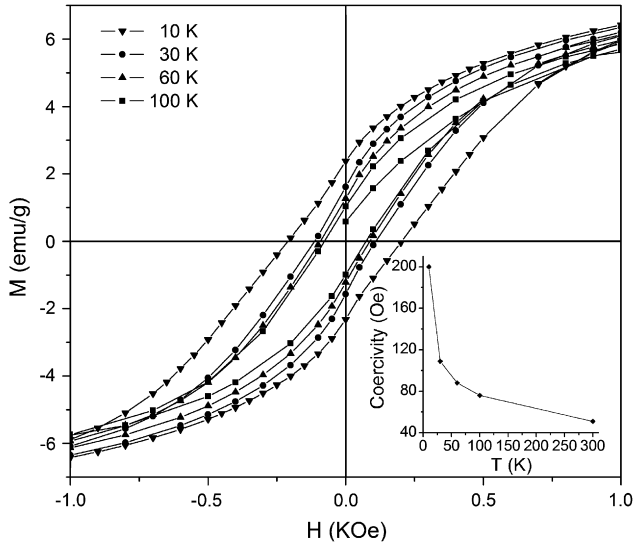

Fig. 8. *M–H* curves at different temperatures of the composite with four deposition cycles. Inset: coercivity field obtained at different temperatures.

temperature, as expected. Although iron oxide particles below 20 nm diameter commonly show a superparamagnetic behavior at room temperature [13,14], in this case, the coercivity field is possibly related to the presence of two magnetic phases [44]. These results are consistent with the weak ferrimagnetic behavior observed in magnetic bacterial cellulose membrane, due to the presence of different iron compounds [13]. In order to study the magnetic behavior at different magnetic field intensities of the resulting composite, ZFC and FC magnetization curves at low and high magnetic fields were carried out. The irreversible magnetization is quite high at low magnetic field intensity, as can be observed in Fig. 9a. However, as the magnetic field was increased, the irreversibility started to close and was only observed at low temperatures. Fig. 9b shows this effect when a magnetic field of 1000 Oe was applied. The observed increase

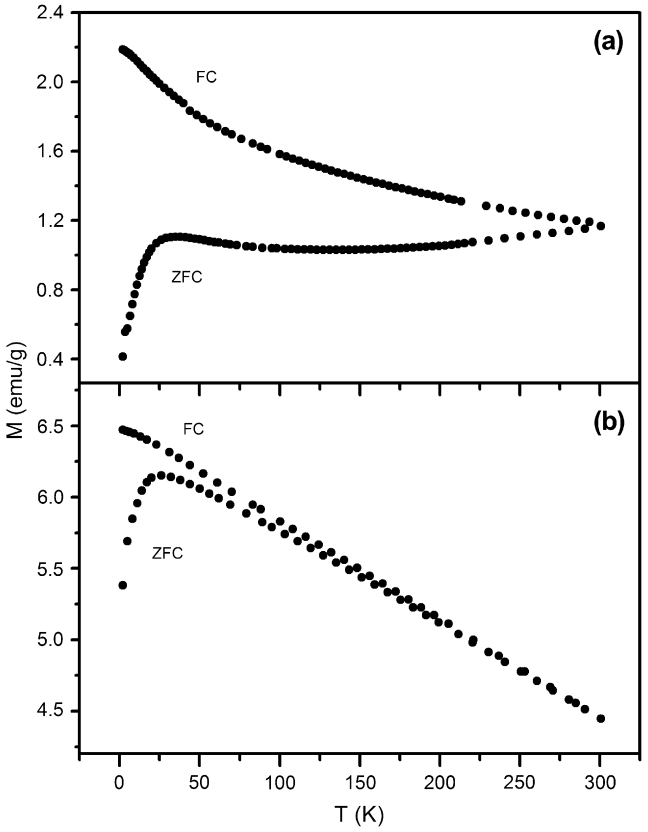

Fig. 9. ZFC and FC magnetization curves of the composite after four deposition cycles measured at (a) 100 Oe and (b) 1000 Oe.

in the M_{ZFC} from 0.4 emu/g to 5.4 emu/g for 100 Oe and 1000 Oe of applied magnetic field, respectively, is indicative of a weak ferrimagnetic ordering, related to spin alignments in preferred directions [44]. In addition, the M_{ZFC} values reach a maximum, which are associated with the blocking temperature T_b of superparamagnetic particles. In this system, T_b is about 26 K; below this temperature the coercivity increased drastically due to changes in the magnetic behavior of the particles from superparamagnetism to ferrimagnetism.

4. Conclusions

A magnetic composite was prepared by in situ precipitation of iron oxide using a *N*-carboxyalkyl-maleimide cross-linked copolymer as template. FTIR and XPS analyses showed sodium carboxylate formation in the cross-linked copolymer after the iron oxide deposition treatment. The evolution of iron content with the number of deposition cycles showed a drastic increase due to higher absorption of iron ions by the cross-linked copolymer with sodium carboxylate groups. The deposited iron oxide phase after the third deposition cycle was identified as a mixture of goethite and maghemite by XRD analyses. TEM micrographs showed spherical particles inside the polymer matrix. After the fourth deposition cycle, formation of aggregates was observed due to nonstoichiometric iron oxide deposition. The magnetic properties of the resulting composite reached a maximum after the third deposition cycle.

The resulting composite showed a coercivity field at room temperature, due to the presence of two magnetic phases, indicating the potential value for technological applications in magnetic storage devices.

Acknowledgments

The authors thank Jesús Antonio Díaz and Francisco Ruiz (CCMC – UNAM) for technical assistance in XPS and HRTEM measurements, respectively, Maricela Garcia-Zamora for FTIR measurements and Jose A. Sanchez for elemental analyses. S. Sepúlveda-Guzmán also acknowledges CONACyT for a doctoral scholarship. This work was financed by CONACyT project C25422-A.

References

[1] Dong-Hwang C, Shih-Hung H. Process Biochem 2004;39(12):2207–11.
[2] Neuberger T, Schöpf B, Hofmann H, Hofmann M, Rechenberg Bv. J Magn Magn Mater 2005;293(1):483–96.
[3] Cumbal L, Greenleaf J, Leun D, SenGupta AK. React Funct Polym 2003; 54(1–3):167–80.
[4] Petri-Fink A, Chastellain M, Juillerat-Jeanneret L, Ferrari A, Hofman H. Biomaterials 2005;26(15):2685–94.
[5] Sourty E, Ryan DH, Marchessault RH. Chem Mater 1998;10(7):1755–7.
[6] Peikov VT, Jeon KS, Lane AM. J Magn Magn Mater 1999;193(1–3): 307–10.
[7] Xu X, Friedman G, Humfeld KD, Majetich SA, Asher SA. Chem Mater 2002;14(3):1249–56.
[8] Wang M, Singh H, Hatton TA, Rutledge GC. Polymer 2004;45(16): 5505–14.
[9] Govindaraj B, Sastry NV, Venkataraman A. J Appl Polym Sci 2004; 93(2):778–88.
[10] Raymond L, Revol JF, Marchessault RH, Ryan DH. Polymer 1995; 36(26):5035–43.
[11] Marchessault RH, Rioux P, Raymond L. Polymer 1992;33(19):4024–8.
[12] Raymond L, Revol J-F, Ryan DH, Marchessault RH. Chem Mater 1994; 6(2):249–55.
[13] Sourty E, Ryan DH, Marchessault RH. Cellulose 1998;5(1):5–17.
[14] Ziolo RF, Giannelis EP, Weinstein BA, O'Horo MP, Ganguly BN, Mehrotra V, et al. Science 1992;257(5067):219–23.
[15] Sohn BH, Cohen RE. Chem Mater 1997;9(1):264–9.
[16] Ahmed SR, Kofinas P. Macromolecules 2002;35(9):3338–41.
[17] Ru-Jong J, Chia-Cheng C, Chih-Ping C, Chin-Ti C, Wen-Chiung S. Polymer 2003;44(1):143–55.
[18] Matsumoto A, Kubota T, Otsu T. Macromolecules 1990;23(21): 4508–13.
[19] Patel DK, Patel CG, Parmar JS. Macromolecular Rep 1994;A31: 297–307.
[20] Knaus S, Liska A, Sulek P. J Polym Sci A Polym Chem 2003;41(21): 3400–13.
[21] Kohli P, Blanchard GJ. Langmuir 2000;16(22):8518–24.
[22] Pérez-Camacho O, Sepúlveda-Guzmán S, Pérez-Alvarez M, García-Zamora M, Cadenas-Pliego G. Polym Int 2005;54(12):1626–31.
[23] Reagent chemicals: American chemical society specifications. 5th ed. Washington: American Chemical Society; 1974. p. 17–8.
[24] Moulder JF, Stickle WF, Sobol PE, Bomben KD. Handbook of X-ray photoelectron spectroscopy. Minnesota, USA: Perkin–Elmer Corporation, Physical Electronics Division; 1992.
[25] Sepúlveda-Guzmán S, Pérez-Camacho O, Rodríguez-Fernández O, García-Zamora M. J Magn Magn Mater 2005;294(2):e47–50.
[26] Kroll E, Winnik FM, Ziolo RF. Chem Mater 1996;8(8):1594–6.
[27] Kim DK, Mikhaylova M, Zhang Y, Muhammed M. Chem Mater 2003; 15(8):1617–27.
[28] Shen G, Anand MFG, Levicky R. Nucleic Acids Res 2004;32(20): 5973–80.
[29] Liu G, Li X, Zhang L, Qu X, Liu P, Yang L, et al. J Appl Polym Sci 2002; 83(2):417–22.
[30] Morjan I, Alexandrescu R, Soare I, Dumitrache F, Sandu I, Voicu I, et al. Mater Sci Eng C 2003;23(1–2):211–6.
[31] Sudakar C, Subbanna GN, Kutty TRN. J Phys Chem Solids 2003;64(12): 2337–49.
[32] Powder diffraction file data base, International Centre for Diffraction Data 1993C.
[33] Frost R, Zhu HY, Wu P, Bostrom T. Mater Lett 2005;59(17):2238–41.
[34] Veiga V, Ryan DH, Sourty E, Llanes F, Marchessault RH. Carbohydr Polym 2000;42(4):353–7.
[35] Beamson G, Briggs D. High resolution XPS of organic polymers. New York, NY: John Wiley & Sons; 1992. p. 293.
[36] Alexander MR, Beamson G, Blomfield CJ, Leggett G, Duc TM. J Electron Spectrosc Relat Phenom 2001;121(1–3):19–32.
[37] Tan BJ, Klabunde KJ, Sherwood PMA. Chem Mater 1990;2(2):186–91.
[38] McIntyre NS, Zetaruk DG. Anal Chem 1977;49(11):1521–9.
[39] Yin X, Stöver HDH. Macromolecules 2002;35(27):10178–81.
[40] Deng J, He C, Peng Y, Wang J, Longa X, Li P, et al. Synth Met 2003; 139(2):295–301.
[41] Morais PC, Azevedo RB, Silva LP, Rabelo D, Lima ECD. Phys Status Solidi 2001;187(1):203–7.
[42] Banfield JF, Welch SA, Zhang H, Ebert TT, Penn RL. Science 2000; 289(5480):751–4.
[43] Winnik FM, Moreau A, Ziolo RF, Stöver HDH, Li W-H. Langmuir 1995; 11(10):3660–6.
[44] Joy PA, Kumar PSA, Date SK. J Phys Condens Matter 1998;10(48): 11049–54.